Investigation of Wire Effect in Sub-channels for 7-Pin Fuel Assembly

J. H. Jeong [a*], J. Yoo [a], K. L. Lee [a], K. S. Ha [a]

[a] Korea Atomic Energy Research Institute, 989-111, Daedeok-daero, Yuseong-gu, Daejeon, 305-353
[*]Corresponding author: jhjeong@kaeri.re.kr

1. Introduction

The wire effect on three-dimensional flow field and heat transfer characteristics in a helically wrapped 7-pin fuel assembly mock-up of an SFR (Sodium-cooled Fast Reactor) have been investigated through a numerical analysis using the commercial CFD (Computational Fluid Dynamics) code, CFX.

The SFR system has a tight package of the fuel bundle and a high power density. The sodium material has a high thermal conductivity and boiling temperature than the water. That can make core design to be more compact than LWR (Light Water Reactor). The fuel assembly of the SFR system consists of long and thin wire-wrapped fuel bundles and a hexagonal duct, in which wire-wrapped fuel bundles in the hexagonal duct has triangular array. The main purpose of a wire spacer is to avoid collisions between adjacent rods. Furthermore, a vortex induced vibration can be mitigated by wire spacers. The wire spacer can enhances a convective heat transfer due to the secondary flow by helically wrapped wires.

In this study, complicated and separated flow phenomena in the 7-pin fuel assembly without wire spacer and with wire spacer were captured by a RANS (Reynolds-Averaged Navier-Stokes) flow simulation with the SST (Shear Stress Transport) turbulence model, and by the vortex structure identification technique based on the critical point theory.

2. Numerical Analysis Methodology

2.1 Test Section

A numerical study of the 7-pin fuel assembly was carried out in the sodium boiling and fuel failure propagation test loops (SIENA) installed at PNC's Oarai engineering center. The geometric parameters of the 7-pin fuel assembly are summarized in Table 1. [1]

Figure 1 shows a schematic of the test section and an cross sectional view of the fuel assembly with wire spacers. As shown in Table 1 and Fig. 1, an electrically heated 7-pin bundle was centered in a hexagonal duct, with a 23.6 mm flat-to-flat distance inside. The heated pins were 6.5 mm in diameter with 0.55 mm cladding thickness, arranged in a triangular array with a pin pitch of 7.9 mm, and had a 450 mm heated length. 7 pins of 6.5 mm in diameter were wrapped by wire spacers of 1.3 mm in diameter with a wrapping lead of 264.8 mm. The pitch-to-diameter ratio (P/D) was 1.22.

Table 1. Test section geometric parameters of 7-pin with wire

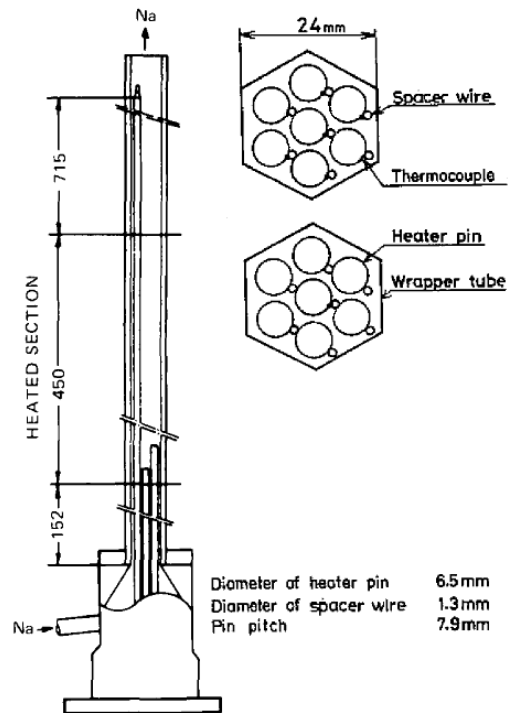| Geometric parameters	Value
Number of pins	7
Pin diameter (mm)	6.5
Pin pitch (mm)	7.9
Pitch-to diameter ratio	1.22
Pin length (mm)	1317
Heated length (mm)	450
Heat flux distribution	Uniform
Duct inner flat-to-flat distance (mm)	23.6
Wire spacer diameter (mm)	1.3
Wire lead pitch (mm)	264.8
Cladding thickness (mm)	0.55

Fig. 1. Schematic of the test section [2]

2.2 Test Section of Numerical Analysis

The present CFD investigation was carried out over the full-scale experimental facility of SIENA's 7-pin fuel assembly. Figure 2 shows the test section of the numerical analysis and duct wall surface with red color on the heated location of the hexagonal duct.
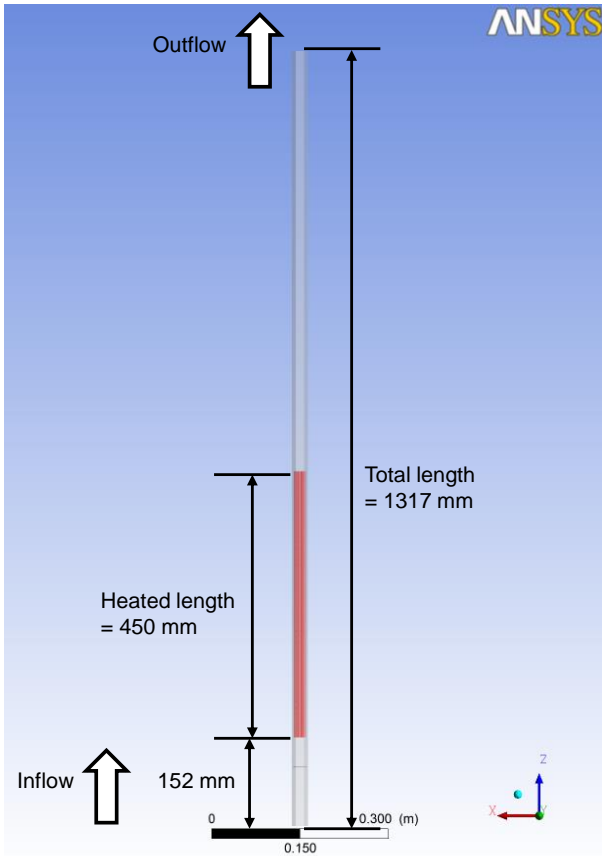
Fig. 2. Normalized axial velocity at 500mm from inlet

Table 2. The geometric parameters of 7-pin without wire

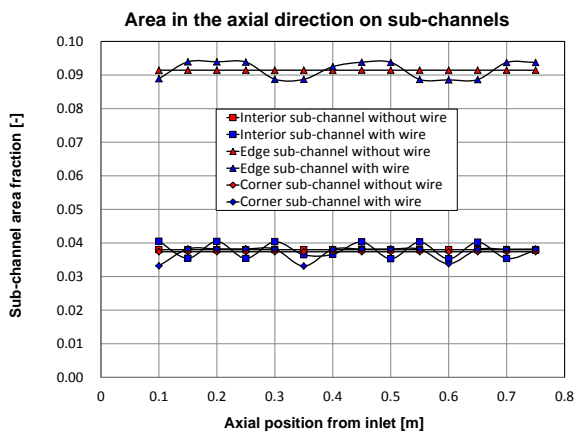| Geometric parameters	Value
Number of pins	7
Pin diameter (mm)	6.629
Pin pitch (mm)	7.9
Pitch-to diameter ratio	1.192
Pin length (mm)	1317
Heated length (mm)	450
Heat flux distribution	Uniform
Duct inner flat-to-flat distance (mm)	23.6

Fig. 3. Sub-channel area fraction with axial position from inlet

To understand heat transfer characteristics due to wire spacer, the numeric analysis of the 7-pin fuel assembly without wire is also conducted. In case of the CFD analysis without wire, the geometric parameters of the 7-pin fuel assembly are as following table 2. The pin diameter without wire is larger than that with wire. Figure 3 shows sub-channel area fraction with axial position from inlet region. Sub-channel area fraction value is axially fluctuating because helically wrapped wire spacers periodically pass through certain sub-channels.

2.3 Computational Grids and Boundary Conditions

Figure 4 shows the cross sectional view with grid distribution, which is divided into interior (red and yellow color), edge (green color), and corner (blue color) sub-channels. All sub-channels are numbered 1 through 18 in a clockwise and radial direction. Figs. 4 (a), (b) are the 7-pin fuel bundles without wire spacers and with wire spacers, respectively. Both computational grid systems of the 7-pin fuel assembly are composed of hexagonal meshes. As shown in Fig. 4, all fuel bundles are numbered 1 through 7 clockwise. Compared to other studies [3-6] with a trimmed shape at the interface between pin surface and wire surface, this RANS based flow simulation is carried out without any trimmed shapes in this study.
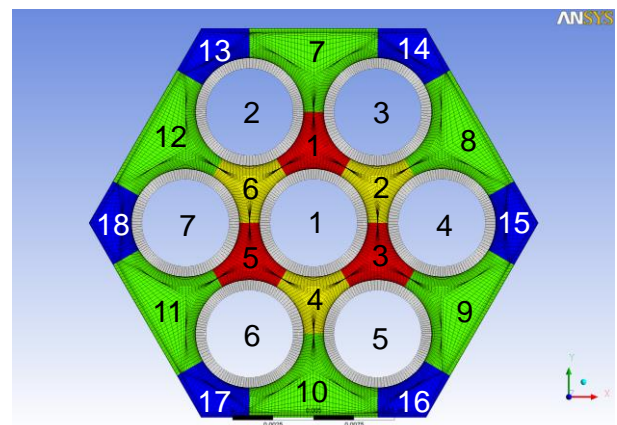
(a) Without wire
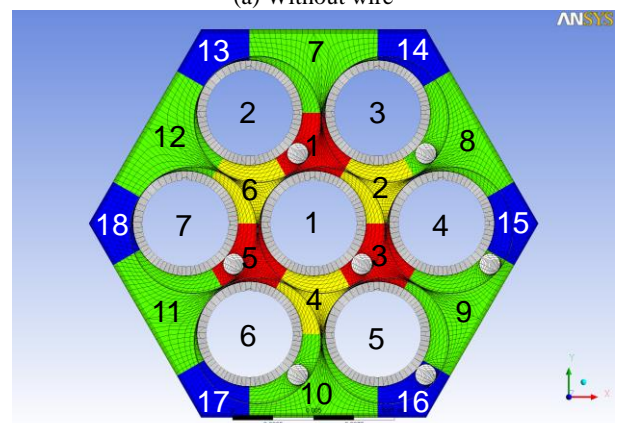
(b) With wire

Fig. 4. Cross sectional view with grid distribution

Table 3 describes the computational grids system. The computational grid system is divided into two regions: a fluid part and a structure part. The total number of computational grids in the system was approx. 2.78×10^6 cells.

Table 3. Computational grid system

7-Pin	Cells	Nodes	Elements
Fluids	1,583,790	1,646,330	1,583,790
Structures	1,192,100	1,341,340	1,192,100
Total	2,775,890	2,987,670	2,775,890

Table 4 describes the computational boundary condition of the CFD analysis. The inlet and outlet are defined with various velocities, a temperature of 556.25 K, and a relative pressure of 0 Pa. The inner cladding domain of the heated section has a constant heat flux of 660198 W/m^2. The outer claddings and wire spacers are defined with no slip condition, conservative interface flux, and smooth roughness. The duct wall is applied under no slip and adiabatic conditions.

Table 4. Boundary condition in the 7-pin fuel assembly

Boundary domain	Condition	Value
-Inlet	-Constant velocity [m/s]	1.3059 1.6685 2.1711 2.6995
-Outlet	-Relative pressure [Pa]	0
-Inner cladding	-Constant heat flux [W/m^2]	660198
-Rod & wire outer	-No slip (Smooth wall)	-
-Duct Wall	-No slip (Adiabatic)	-

2.4 Turbulence Model

Three major numerical analysis techniques can be used for turbulent flow fields: DNS (Direct Numerical Simulation), LES (Large Eddy Simulation), and RANS (Reynolds-averaged Navier-Stokes) simulation. In order to precisely analyze the general vortex behavior in a turbulent flow field containing vortices of various scales, it is necessary to make the calculation grid size smaller than the minimum space scale of the vortex structure and the time interval less than the minimum time scale of the vortex variation. Assuming that computing the cost of the RANS is equal to one, that of the DNS and LES increases as the cube and square of the Reynolds number, respectively. The Reynolds number based on the averaged axial velocity and the hydraulic diameter of the present fuel assembly is higher than 1.29×10^4. For this reason, the DNS and LES are not feasible methods for the full-scale 7-pin fuel assembly of the test section. RANS is a very practical and affordable engineering solution with good knowledge of the turbulence.

The turbulence models for the RANS equations are for computing the Reynolds stresses tensor from turbulent fluctuations in the fluid momentum. Turbulence models such as the *k-ε*, *k-w*, and SST have become industry standard models and are commonly used for most types of engineering problems, although the *k-ε* model has the weakness in cases of large adverse pressure gradient, and the *k-w* model is too sensitive to the inlet free-stream turbulence properties (Wilcox et al. [7]). The SST model solves the above problems for switching to the *k-ε* model in the free-stream and the *k-w* model in the viscous sub-layer (Menter et al. [8]). The minimum grid scale on the fuel rod surface was 5.0×10^{-7} mm to capture the laminar to turbulent flow transition with the SST turbulence model; the friction velocity y* is approximately close to 1.

In the present study, we conducted the steady RANS simulation with the SST turbulence model for investigating the three-dimensional and vortical flow phenomena. The high-resolution scheme was used for the convective term. Convergence of the simulation was judged by the periodic pressure and temperature on the outlet domain of the 7-pin fuel assembly.

2.5 Grid Sensitivity Study

The CFD analysis results with the SST turbulence model are very dependent on the wall y* grid scale of the wire-wrapped fuel bundle surface. A dependency study of the wall y* grid scale was carried out using the 7-pin fuel assembly with wire spacer. Figure 5 depicts the friction factor with a different wall grid scale in a wire-wrapped 7-pin fuel assembly. As shown in Fig. 5, friction factor uncertainties with different wall grid spacing was under 6.0 %. Figure 6 shows the residual RMS (Root Mean Square) value time history of pressure. As shown in Fig. 6, the pressure RMS value with time is not dependent on the wall grid spacing.
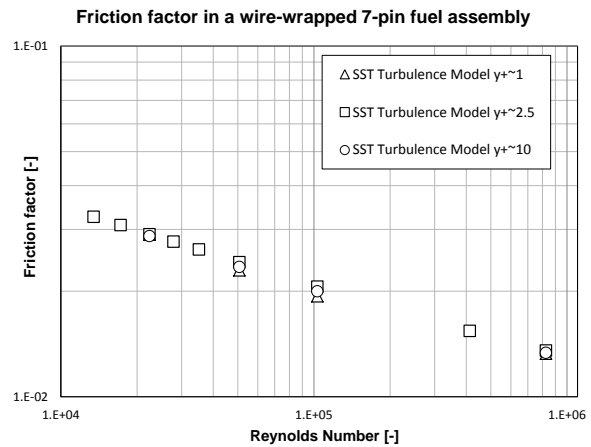

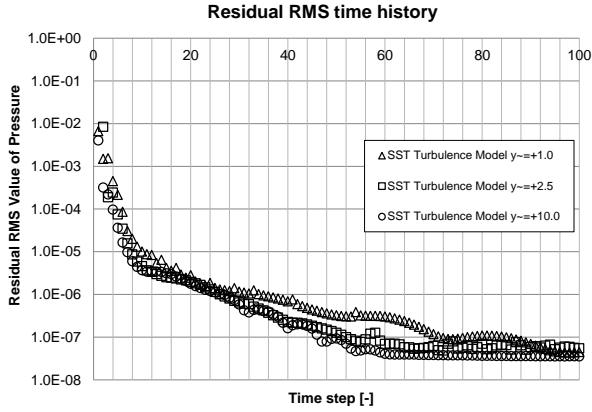Fig. 5. Friction factor with different wall grid scales in the wire-wrapped 7-pin fuel assembly

Fig. 6. Residual RMS value time history of pressure in the wire-wrapped 7-pin fuel assembly

3. Numerical Analysis Results

3.1 Comparison of Pressure Drop Correlations

Friction factor correlations such as the Rehme model [9], Engel et al. model [10], and Cheng and Todreas simplified model [11] have been widely used for the wire-wrapped fuel bundle. Each friction factor is calculated through the following correlations.

- Rehme model

$$f = \frac{64}{Re} \cdot F^{0.5} + \frac{0.0816}{Re^{0.1333}} \cdot \frac{N_r \cdot \pi \cdot D_r + D_w}{S_t} \qquad (1)$$

- Engel, Markley and Bishop model

Laminar flow: $f = \dfrac{110}{Re}$ for $Re \leq 400$,

Turbulent flow: $f = \dfrac{0.55}{Re^{0.25}}$ for $Re \geq 5000$, $\qquad (2)$

Transition flow: $f = \dfrac{110}{Re} \cdot \left(1 - \psi\right)^{0.5} + \dfrac{0.55}{Re^{0.25}} \cdot \psi^{0.5}$

for $400 \leq Re \leq 5000$,

- Cheng and Todreas simplified model

Laminar flow: $f = \dfrac{C_{fL}}{Re}$ for $Re \leq Re_L$,

Turbulent flow: $f = \dfrac{C_{fT}}{Re^{0.18}}$ for $Re_T \leq Re$, $\qquad (3)$

Transition flow: $f = \dfrac{C_{fL}}{Re} \cdot \left(1 - \psi\right)^{1/3} + \dfrac{C_{fT}}{Re^{0.18}} \cdot \psi^{1/3}$

for $Re_L \leq Re \leq Re_T$,

Figure 7 depicts a comparison of the CFD analysis results with friction factor correlations of the Rehme model, Engel et al. model, and Cheng and Todreas simplified model in various ranges of Reynolds number. As shown in Fig. 7, the Cheng and Todreas model has a good agreement with the CFD.

Figure 8 shows the axially distributed friction factors. The friction factor near the inlet region is also over-estimated until the inlet flow reaches about the end position of one or two periodical wire lead pitch. To calculate the friction factor without numerical boundary effect of inlet region, at least two or third periodical wire lead pitches should be modeled in the CFD simulation to prevent an over-estimation of the friction factor.
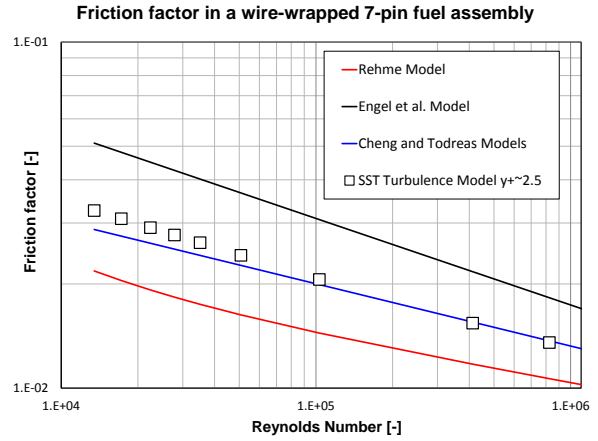

Fig. 7. Comparison of the CFD results with friction factor correlations in various range of Reynolds number
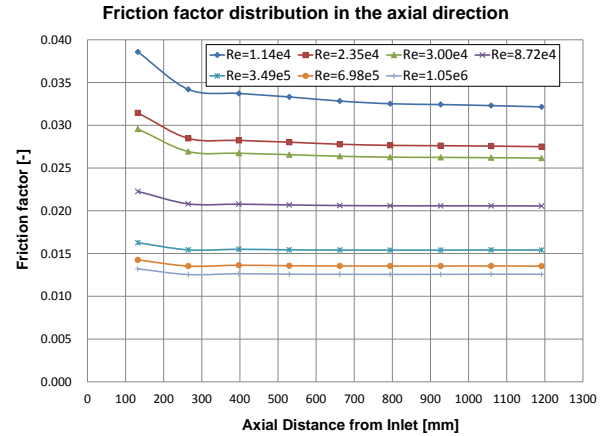

Fig. 8. Axially distributed friction factor in various range of Reynolds number

3.2 Comparison of Heat Transfer Correlations

A thermal energy from a fission of the fuel pins is transferred to the coolant by the convection. In case of SFR, the coolant is sodium which has higher transfer coefficients than other fluid. However, for many fluids, including water, Pr (Prandtl number) lies in the range from 1 to 10. For gases, Pr is generally about 0.7. For sodium, the Prandtl number is very small, generally in the range under 0.01. [12] This means that the mechanisms of conductive heat transfer dominate over those of momentum transfer in sodium. Typical Peclet numbers for normal operation are from 150 to 300 in the fuel assemblies.

Borishanskii et al. [13] and Graber et al. [14] proposed the following correlations.

- Borishanskii et al. model

$$Nu = 24.15 \log_{10} \left[-8.12 + 12.76 \ \frac{P}{D} - 3.65 \ \frac{P}{D} \right] \quad (4)$$

For $1.1 \leq P/D \leq 1.5$ and $Pe \leq 200$.

- Graber and Rieger model

$$Nu = 0.25 + 6.2 \ \frac{P}{D} + \left[0.32 \ \frac{P}{D} - 0.007 \right] Pe^{\ 0.8 - 0.024 \ P/D} \quad (5)$$

For $1.25 \leq P/D \leq 1.95$ and $150 \leq Pe < 3000$.

The most of turbulence models using an eddy diffusivity concepts use a turbulent Prandtl number (Pr_t) to describe the turbulence heat transport. In case of conventional fluids such as water and air, a constant Pr_t of about 0.9 is widely used, and the value is based on the experimental evidences. To simulate turbulent energy transfer, the Reynolds analogy approach [15] is usually applied in conventional fluids. However, the value of the Pr_t may not be valid for sodium coolant. In case of liquid metal, Pr_t is greater than unity and decreases with increasing Reynolds number and distance from the wall. [16] This phenomenon is opposite to the air. [17] Pr_t of the air is less than one, and increases towards unity with increasing Reynolds number and distance from the wall. Prandtl number in the CFD analysis is generally determined as below.

$$\mu = \mu_l + \mu_t \quad (6)$$

$$\frac{\mu}{Pr} = \frac{\mu_l}{Pr_l} + \frac{\mu_t}{Pr_t} \quad (7)$$

An eddy viscosity is calculated by a turbulence model, and then, Prandtl number is determined by equation (7). Figure 9 depicts the Nusselt number of the CFD analysis results with different Pr_t in various range of Peclet number. As shown in Fig. 9, the CFD analysis results with Pr_t of 0.02 have a good agreement with Borishanskii et al. model and Graber and Rieger model. The increase of the Pr_t leads to the decrease of heat transfer as shown in Fig. 9.

Nusselt number of the 7-pins with wire spacer is about 50 % higher than that without wire spacer. The wire spacer enhances the heat transfer characteristics
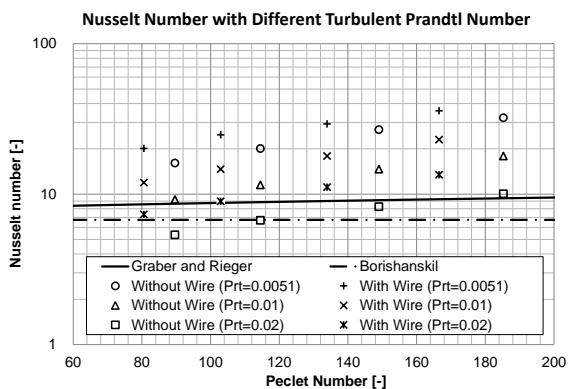
Fig. 9. Heat transfer comparison of correlations and the CFD results with different Pr_t in various range of peclet number

3.3 Three-dimensional Analysis

The three-dimensional flow field with Pr_t of 0.02 has been investigated at a Peclet number of about 1.8×10^3. Figure 10 shows the axial velocity distribution normalized by inlet velocity on the planes of 400, 500, and 600 mm, which are perpendicular to the axial direction. Figs. 10 (a) and (b) are without wire, and with wire, respectively. Both of axial velocities on the edge and corner sub-channels are higher than that on the
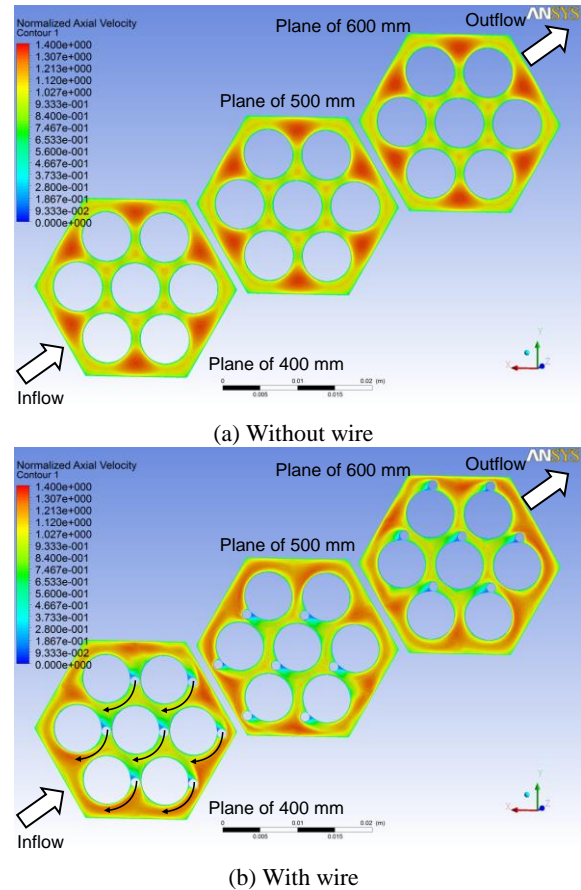
(a) Without wire

(b) With wire

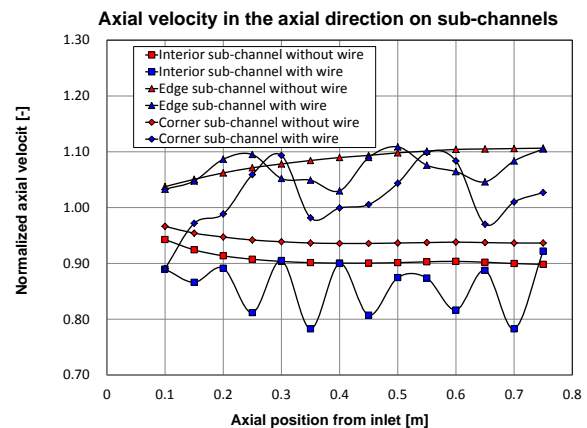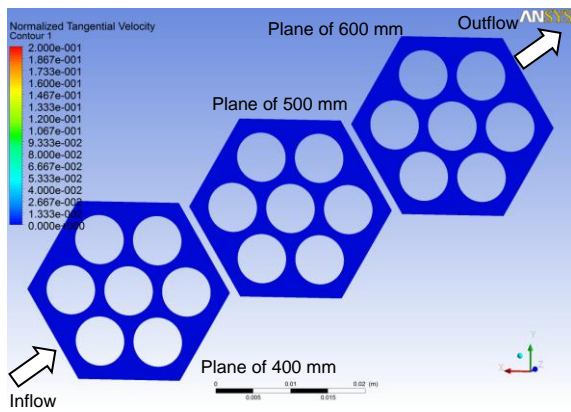Fig. 10. Axial velocity distribution normalized by inlet velocity

Fig. 11. Normalized axial velocity by inlet velocity on the sub-channels with axial position from inlet

interior sub-channels. In case with wire, wake regions due to helically wrapped wire spacers are developed nearby the suction surface of wire spacers.
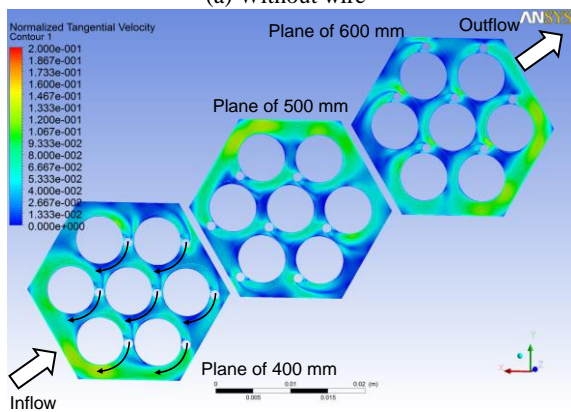
Figure 11 depicts the normalized axial velocity averaged in each sub-channel area with axial position from inlet. The axial velocity of the interior and edge sub-channel with wire is lower than that without wire. However, the axial velocity of the corner sub-channel with wire is higher than that without wire.

Figure 12 shows the tangential velocity distribution normalized by inlet velocity on the cross sectional planes of 400, 500, and 600 mm axial position. Figs. 12 (a) and (b) are without wire, and with wire, respectively. The wire spacers induce a tangential flow by up to about 13 % of the axial velocity. The tangential flow in the corner and edge sub-channels is much stronger than that in the interior sub-channels. The flow with a high tangential velocity is periodically rotating in a period of wire lead pitch.

Figure 13 shows the normalized temperature distribution by inlet temperature on the cross sectional planes of 400, 500, and 600 mm height with local range contour. Figs. 13 (a) and (b) are without wire, and with wire, respectively. The peak temperature of 7-pins with wire is located at the connected interface region between center-pin and wire, and helically rotating with wire spacer. The region with peak temperature is corresponding to the wake region due to wire spacer in Fig. 10. As shown in Fig. 13, heat transfer in case with

wire spacer is significantly enhanced because of the tangential flow due to wire spacer. Figure 14 depicts the normalized temperature averaged in each sub-channel area with axial position from inlet. The temperature of the interior sub-channel with wire is lower than that without wire. However, the temperature of the edge and corner sub-channel with wire is almost higher than that without wire. Those phenomena due to the wire spacer make the strong cross flow over the interior, edge, and corner sub-channels. As it has been mentioned before, the tangential flow due to the wire spacer can achieve to enhance heat transfer characteristics up to about 50 %.
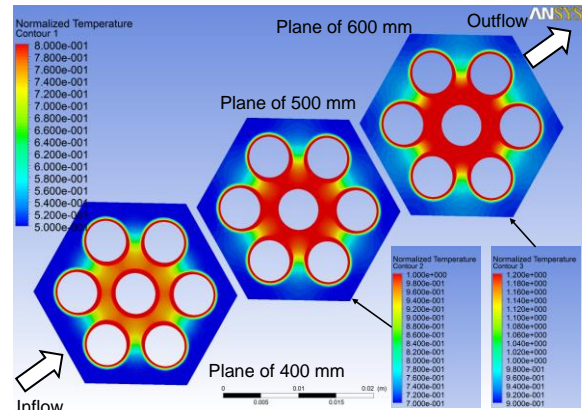
(a) Without wire
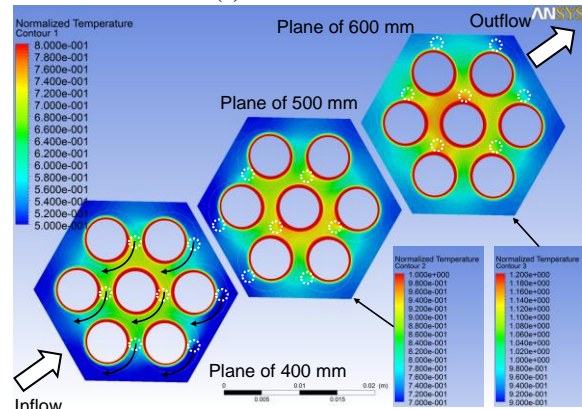
(b) With wire
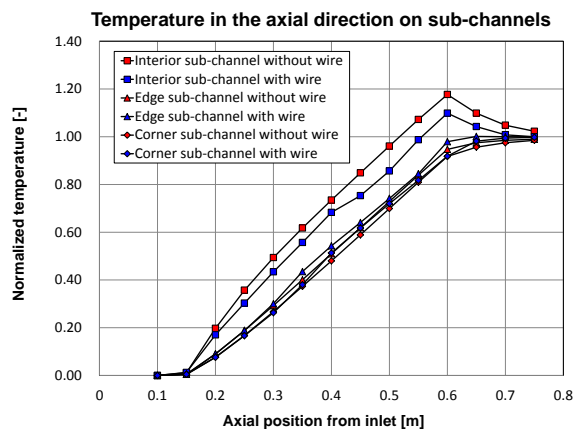
Fig. 13. Normalized temperature distribution

(a) Without wire

(b) With wire

Fig. 12. Normalized tangential velocity distribution

Fig. 14. Normalized temperature distribution

4. Conclusions

The wire effect on three-dimensional flow field and heat transfer characteristics in a helically wrapped 7-pin fuel assembly mock-up of the SFR have been investigated through a numerical analysis using the commercial CFD code, CFX. Complicated and separated flow phenomena in the 7-pin fuel assembly without wire spacer and with wire spacer were captured by the RANS flow simulation with the SST turbulence model.

It is concluded that the wire spacers locally induce a tangential flow by up to about 13 % of the axial velocity. The tangential flow in the corner and edge sub-channels is much stronger than that in the interior sub-channels. The flow with a high tangential velocity is periodically rotating in a period of wire lead pitch. The cross flow due to the wire spacer can achieve to enhance heat transfer characteristics up to about 50 %.

REFERENCES

[1] Y. Daigo et al., Local Temperature Rise due to a 6—Channel Blockage in a 7-Pin Bundle, JAPFNR-202, 1975.
[2] K. Haga et al., The Effects of Bowig Distortions on Heat Transfer in a Seven-pin Bundle, ASME Winter Annual Meeting, New York, NY,1974.
[3] I. Ahmad, K.Y. Kim, Flow and convective heat transfer analysis using RANS for a wire-wrapped fuel assembly, Journal of Mechanical Science and Technology, 20, pp. 1514-1524, 2006.
[4] R. Gajapathy, K. velusamy, P. Selvaraj, P. Chellapandi, and S.C. Chetal, CFD investigation of helical wire-wrapped 7-pin fuel bundle and the challenges in modeling full scale 217 pin bundle, Nuclear Engineering and Design, 237, pp. 2332-2342, 2007.
[5] W. Raza, K.Y. Kim, Shape optimization of wire-wrapped fuel assemblyy using Kriging metamodeling technique, Nuclear Engineering and Design, 238, pp. 1332-1341, 2008.
[6] P.F. Fischer, A. Siegel, and P. Palmiotti, Large eddy simulation of wire wrapped fuel pins Ⅰ: Hydrodynamics in a periodic array, Proceedings of M&C + SNA 2007, Monterey, California.
[7] D. C. Wilcox, Reassessment of the Scale-determining Equation for Advanced Turbulence Models, AIAA Journal, 26(11), pp.1299-1310, 1998.
[8] F. R. Menter, Two-equation eddy-viscosity turbulence models for engineering applications, AIAA Journal, 32(8), pp. 1598-1605, 1994.
[9] K. Rehme, Pressure Drop Correlations for Fuel Element Spacers, Nuclear Technology, 17, pp. 15-23, 1973.
[10] F. C. Engel, R. A. Markley, and A. A. Bishop, Laminar, Transition, and Turbulent Parallel Flow Pressure Drop Across Wire-wrap-spaced Rod Bundles, Nuclear science and engineering, 69, pp. 290-296, 1979.
[11] S. K. Cheng and N. E. Todreas, Hydrodynamic Models and Correlations for Bara and Wire-wrapped Hexagonal Rod Bundles-bundle Friction Factors, Sub-channel Friction Factors and Mixing Parameters, Nuclear Engineering and Design, 92, pp. 227-251, 1986.
[12] A.E. Waltar, Fast Breeder Reactors, PERGAMON PRESS.
[13] V.M. Borihanskii, M. A. Gotovskii, and E.V. Firsova, Heat Transfer to Liquid Metal Flowing Longitudinally in Wetted Bundle Rods, Atomic Energy, 27, pp. 549-568, 1969.
[14] H. Graber, and M. Rieger, Experimental Study of Heat Transfer to Liquid Metals Flowing In-line through Tube Bundles, Progress in Heat Mass Transfer, 7, pp.151-166, 1973.
[15] A.J. Renolds, The Prediction of Turbulent Prandtl and Schmidt Numbers, International Journal of Heat and Mass Transfer, 18, pp. 1055-1069, 1975.
[16] A.D. Carr, R.E. Balzhiser, Temperature Profiles and Eddy Diffusivities in Liquid Metals, Birt. Chem. Eng., 12, pp. 227, 1967.
[17] C.A. Sleicher, J.R. Emeryville, and Calif, Experimental Velocity and Temperature Profile for Air in Turbulent Pipe Flow, Trans. ASME, pp. 693, 1958.